Cyclic swelling enabled, electrically conductive 3D porous structures for microfluidic urinalysis devices

Mengtian Yin[a], Wanqing Xie[b], Li Xiao[b], Sun-Sang J. Sung[c,d], Mingyang Ma[e], Li Jin[b], Xudong Li[b]*, Baoxing Xu[a]*

[a]Department of Mechanical and Aerospace Engineering, University of Virginia, PO Box 400746 122 Engineer's Way, Charlottesville, VA 22904, USA.

[b]Department of Orthopedic Surgery, University of Virginia, 450 Ray C Hunt Dr, Charlottesville, VA 22908, USA.

[c]Division of Nephrology, Department of Medicine, University of Virginia Health Sciences Center, PO Box 800133, Charlottesville, Virginia 22908, USA.

[d]Center for Immunity, Inflammation, and Regenerative Medicine, University of Virginia School of Medicine, PO Box 800133, Charlottesville, VA 22908, USA.

[e]Department of Surgery, University of Virginia, 1300 Jefferson Park Avenue, Charlottesville, Virginia 22908, USA.

*Corresponding author.

E-mail addresses: xl2n@virginia.edu (X. Li), bx4c@virginia.edu (B. Xu)

ABSTRACT

Urinalysis is a simple and non-invasive approach for the diagnosis and monitoring of organ health and also is often used as a facile technique in assessment of substance abuse. However, quantitative urinalysis is predominantly limited to clinical laboratories. Here, we present an electrical sensing based, reusable, cellular microfluidic device that offers a fast urinalysis through quantitative reading of the electrical signals. The spatial soft porous scaffolds decorated with electrically conductive multiwalled carbon nanotubes that are capable of physically interacting with biomarkers in urine are developed through a cyclic swelling/absorption process of soft materials and are utilized to manufacture the cellular microfluidic device. The sensing capability, sensitivity and reusability (via sunlight exposure) of the device to monitor red blood cells, Escherichia coli, and albumin are systemically demonstrated by programming mechanical deformation of porous scaffolds. *Ex vivo* experiments in disease mouse models confirm the diagnosis robustness of the device in comparable results with existing biochemical tests. The full integration of electrically conductive nanomaterials into soft scaffolds provides a foundation for devising bioelectronic devices with mechanically programmable microfluidic features in a low-cost manner, with broad applications for rapid disease diagnoses through body fluid.

Keywords: microfluidic devices, soft porous scaffold, swelling, electrical sensing, urinalyses

1. Introduction

Urine is a representative body fluid with a rich content of biomarkers that help monitor healthy conditions of organs including kidney, bladder and liver [1-5]. Urinalysis is usually taken as a routine screening in hospitals because of the easy and non-invasive collection, and this laboratory-setting based technique yet is time-consuming, high cost and not accessible to publics. For an example, bacterial culture that is required in diagnosis of urinary tract infection may take a few hours to up to several days [6-8]. Several at-home easy-to-use strips have been developed over the past decades to provide timely and fast detection to biomarker substances of urine [9-12]. Most of these strips such as urine strips are based on colorimetric [13-16] or fluorometric technique [17-20] and comprise reagent pads that are functionalized with biochemical groups and exhibit a color change upon interaction with target substances in urine such as glucose, red blood cells, and protein. In the diagnosis of diabetes, for instance, the color change in the strip after being immerged into the urine will indicate a rough concentration of glucose in the urine. However, these strips can only provide qualitative data and are not sensitive enough to detect small changes of urine (i.e., quantitative data) in response to people lifestyle or disease management. The presence of 150 mg/24hr protein in urine will be considered proteinuria that is strongly related with the malfunction of kidneys [21, 22]. Besides, if the screening is abnormal (sometimes results are false positive or negative due to low sensitivity), specific targeted blood testing in labor-intensive settings is required to confirm the diagnosis. To improve sensitivity and stabilize data readout, electrochemical analysis has been employed [23-25]. It relies on the precise labeling and attachment of specific foreign molecules to the reagent electrode pads that chemically respond to urine substances of interest with high sensitivity and selectivity. However, these labeling strategies usually require complex synthesis steps that may potentially alter intrinsic properties of urine compounds [26-29]. Besides, these analysis devices cannot be reused due to the loss of chemical active agents in electrodes upon contact with urine [30, 31].

Here, we present an electrical sensing based, low-cost, cellular microfluidic device that is enabled by soft, porous PDMS materials with full decorations of multiwalled carbon nanotubes (MWCNTs) and demonstrate its high sensitivity and rapid diagnosis of biomarkers in urine. A cyclic swelling/shrink process of PDMS scaffolds is developed to achieve a fully uniform and dense decorations of MWCNTs onto porous PDMS scaffolds that provide an electrical sensing platform to physically interact with biomarkers during urine flow. The electrically conductive PDMS scaffolds obtained exhibit super-hydrophobicity to body fluid, capable of maintaining the stability and containment-free from monitoring environments and

measurement backflow of liquid in urinalysis. The remarkable sensitivity and accuracy of devices are extensively demonstrated in detection and monitoring of commonly existed biomarkers of red blood cells (RBCs), albumin, and *Escherichia coli* (*E. coli*) in urine, and also remain after several cycles of repeated use with a brief exposure to sunlight. In particular, the diagnosis response to mechanical loadings shows the capability of devices to detect and differentiate biomarkers in a mechanically programmable means. The application demonstrations in the models of nephritis and diabetic mice show agreement diagnosis results with parallel clinical laboratory testing and validate the design features and measurement accuracy and reliability of devices in urinalysis. These studies not only establish a new route for the design and manufacturing of microfluidics based portable and low-cost bioelectronic sensors with high reusability for urinalysis, but also offer a foundation for diagnosing body fluid components in a programmable way, where the full integration of spatial porous scaffolds with electronically conductive nanomaterials serves as the basis for guiding accurate electrical sensing and monitoring to biomarkers.

2. Materials and methods

2.1 Preparation of MWCNTs PDMS porous scaffolds

Porous PDMS scaffolds were prepared using sugar cubes (C&H Pure Cane Sugar Cubes, 1x1x1 cm, pore size 500 ± 300 μm, ~75% porosity) as sacrificial templates [32]. PDMS precursor (Sylgard 184 Silicone Elastomer, Dow Corning Corp.) was firstly mixed with MWCNTs (MWCNT, -COOH functionalized, 8–15 nm diameter, 10–15 μm length, 95%, Nanostructured & Amorphous materials, Inc.) was added to the mixture in a 3% concentration (CNTs: PDMS in weight). After robust stirring with a stir bar, cartridge was delivered to an ultrasonicator for at least 3 h with 40 kHz to achieve a homogeneous distribution of MWCNTs in PDMS precursor. The mixture was then degassed with a vacuum chamber. Afterward, curing agent of PDMS was added to the mixture in a ratio of 10:1 by weight, and degassed again. The as-prepared MWCNT-PDMS mixture was poured into a Petri dish with sugar cubes placed on top and sent to a vacuum chamber for 6 h to ensure all PDMS infiltration into the sugar cube template. The Petri dish was then placed in a heating oven at 80°C for PDMS polymerization. Extra PDMS was removed with a razor blade and then put in a conical tube with DI water and ultra-sonicate for 2 h at 50°C to dissolve the sugar scaffold. CPSs were then obtained after rinsed with DI water to remove residual sugar and fully dried at room temperature.

2.2 Decoration of MWCNTs on PDMS scaffolds by swelling/shrinking

CNT dispersions were made in 50 ml conical tubes by mixing 2 mg MWCNTs (Pristine or -COOH functionalized) with 50 ml of DI water, ethanol, 1-propanol, and n-hexane (Sigma-Aldrich). MWCNT dispersions were ultrasonicated for 2 h to ensure homogeneous MWCNTs dispersion. Then previous *PDMS scaffolds* were placed in the tubes of MWCNT dispersion to make them swell and decorate MWCNTs. Ultrasonicator was used to help decoration of MWCNTs for about 20 mins. Swelled *PDMS scaffolds* were delivered to a hood to remove organic solvents with the help of air blow. After sufficient time (around 1 h), *PDMS scaffolds* return to their original volume and 1 cycle of swelling decoration is considered completed. More cycles are achieved by repeating the swelling decoration process. The mass of MWCNTs decorated on *PDMS scaffolds* was calculated by measuring the volume of absorbed organic solvent by each *PDMS scaffolds* (ml) and multiply by the MWCNT concentration of each solvent (mg/ml).

2.3 Electrical resistance and contact angle measurements

Conductive copper foil was attached to two opposite sides of CPS with wires connect to a digital multimeter (National Instrument, USB-4065). Depending on different situation, foils were either attached on the CPS by gently touching or fixed onto the CPS with conductive silver epoxy adhesive (MG Chemicals 8331 Silver Epoxy Adhesive). Static contact angle was measured with the ramé-hart model 250 goniometer. A drop of DI water of 5 µL was placed on the top side of a CPS. Images and angles were recorded with the ramé-hart DROPimage software.

2.4 Mouse red blood cell collection, E. coli growth, and BSA solution preparation

Blood sample was collected from heart of C57B/6J mice for other projects. Eppendorf tube was pretreated with 8% EDTA. The whole blood was diluted with saline solution and centrifuged at 2000 rpm. OP50 *E. Coli* strain was maintained on a Luria Broth (LB) agar plate. A loopful of the culture from the plate was subcultured before each test and transferred into 2 ml of sterile LB media and grown for 6 h at 37°C at 240 rpm. Cells at different concentrations were tested and plated on LB agar plates to evaluate colony forming unit (CFU). Bovine Albumin Serum (A2153, Sigma) was dissolved in PBS at 1mg/ml.

2.5 Mouse nephritis urine collection

The lupus-prone NZM mouse strain originally obtained from Jackson Laboratory (Bar Harbor, ME, USA) was maintained in our vivarium. Nephrotoxic serum (NTS)-induced

nephritis including glomerulonephritis (GN) and proteinuria in NZM mice was induced by a single injection of mouse erythrocyte-adsorbed sheep anti-glomerulus basement membrane (GBM) antiserum prepared as described [33] plus 40 μg CpG 2395 as adjuvant [34, 35]. Urine samples were collected prior injection and on day 3 and day 7 post injection. Urine albumin was measured by ELISA per our established protocol [33]. Animal use and manipulation followed protocols approved by the University of Virginia Institutional Animal Use and Care Committee.

2.6 Mouse diabetic urine collection

The female C57B/6J mouse strain (8-10 weeks old) was obtained from Jackson Laboratory. Mice were injected intraperitoneally with a single dose of streptozotocin (STZ, 200 mg/kg). Blood glucose was confirmed with a AimStrip Plus blood glucose meter kit (Germaine Laboratories INC) one-week post injection. Blood glucose >300 mg/dL after 3 consecutive glucose measurement was considered diabetic. These diabetic mice received islet transplant surgery per established protocol [36]. Blood glucose was confirmed to return to an average value of 150 mg/dL 30 days after surgery. Urine was collected prior to transplant surgery and at 30-day post-surgery.

3. Results and discussion

3.1 Materials, Designs and Fabrication Procedures of Electrically Conductive Soft Porous Scaffolds

Fig. 1a presents a schematic procedure of preparing porous PDMS scaffolds with the decoration of electrically conductive MWCNTs onto porous surfaces. It consists of two main components: preparation of spatial porous PDMS scaffolds with standard sugar-templated method, and attachment of MWCNTs into porous surfaces with a cyclic PDMS swelling/MWCNTs adsorption approach **(see Materials and Methods)**. The successful decorations of MWCNTs will yield the electrical conductance of porous PDMS scaffolds, capable of sensing fluid transports with a quantitative readout of electrical signals, and the key is to achieve a uniform and dense decoration with strong adhesion. Once the porous PDMS scaffold is fabricated, it is dropped into the well-mixed MWCNTs solution, and the porous PDMS scaffold starts to swell with a volumetric expansion. After that, the swollen scaffold is taken out of the solution for drying by naturally evaporating reagents at room temperature, and will shrink back to its original size after complete drying. The microstructural observations of PDMS scaffold (**Fig. 1b**), together with the color change from original white to black, show

6

the presence of MWCNTs after the swelling/shrinking cycle, indicating the successful attachment of MWCNTs onto PDMS porous scaffolds. The MWCNTs decorated PDMS scaffolds here is referred to as CPS. This attachment is further confirmed by the successful measurement of electrical resistance on CPS (**Fig. S1**). The swelling results from the chemical reaction between polymer networks of PDMS materials and MWCNTs solution, and depends on the chemical reagent of MWCNTs solutions. Assume a uniform expansion of PDMS by swelling, we define the swelling ratio Q to characterize the effect of swelling on absorption of MWCNTs. Detailed relationship between swelling ratio and solubility parameter is summarized in **Fig. S4**. Take four representative reagents, water, ethanol, 1-propanol, and hexane as examples, the microstructures of CPS in Fig. 1b show that a larger swelling ratio leads to a denser decoration of MWCNTs on PDMS scaffold because of enhanced contact areas between swollen PDMS scaffold and MWCNTs.

Consider a solution reagent of hexane, the cyclic study of swelling/shrink-induced absorption of MWCNTs has also been conducted. **Fig. 1c** shows that an increased cycle yields attachments of more MWCNTs onto the PDMS scaffold. The intense attachment with the increasing of cycles is also confirmed by a dramatic decrease of the electrical resistance of CPS, as shown in **Fig. S2**. In addition, **Fig. S3** indicates that the weight of PDMS sponges barely increases due to a negligible amount of absorbed MWCNTs compared to PDMS sponge.

3.2 Fundamental characterization and sensing mechanism

Fig. 2a shows the liquid contact angle and electrical resistance of CPS with a different swelling ratio Q, where only one cycle of swelling/shrink was performed to eliminate the effect of cycles, and the liquid was the phosphate buffered saline (PBS) to mimic body liquid. The increase of Q yields a large contact angle but decreases the electrical resistance, consistent with the intensive and dense decoration of MWCNTs in Fig. 1b. With hexane as the swelling reagent, **Fig 2b** presents the influence of swelling cycles on the contact angle and electrical resistance of CPS. An enhanced contact angle and decreased resistance are obtained with the increasing of cycles, which also agrees with microstructural observations with more absorbed MWCNTs in Fig 1c. The analysis also shows that after seven cycles of swelling and shrink, both the electrical resistance and contact angle reach stable, suggesting a full and dense coverage of MWCNTs on porous PDMS scaffold with a superhigh electrical conductance (R = 983.4Ω) and surface hydrophobicity (contact angle = 146.4°). This swelling/shrinking-induced attachment mechanism of MWCNTs can also be utilized to enhance the surface wettability and electrical conductance of PDMS materials or PDMS/MWCNTs composites through a

7

traditional dip-coating approach, as shown in **Fig. S5**. **Fig. 2c** shows the measurement of contact angle and electrical resistance of CPS under a uniaxial compression strain ε, where the electrical resistance of CPS was measured without liquid droplet on it. The compression strain ε is defined as the (d-d')/d, where d is the side length of the CPS and d' is the length after compression. The large mechanical compression ε is, the higher contact angle and lower resistance are because the compression condenses the distribution of MWCNTs on PDMS scaffolds, similar to those effects of swelling ratio and cycles in Fig.2b. Cyclic compression experiments on CPS under different compressive forces were further performed. The dynamic monitoring of electrical resistance (**Fig. 2d**) shows that CPS remains a full recovery after as high as a 90% compression strain, suggesting a stable attachment of MWCNTs on PDMS scaffolds. This stability of MWCNTs attachment is also confirmed by an unchanged contact angle of CPS after compression, as shown in **Fig. S6a**. Particularly, the experiments on a fatigue loading (**Fig. S6b**) indicates that the resistance only shows a slight drift after 150 cycles under compressive force of 500 N.

To investigate the responsive ability of CPS to biomarkers, red blood cells (RBCs), *Escherichia coli* (*E. coli*), and albumin that are typical diagnostic substances in urine of urinary tract infection and kidney diseases were considered and tested. Bovine serum albumin (BSA), is selected as an accessible source of albumin for testing. These biomarkers were all diluted with phosphate-buffered saline (PBS) solution in multiples of 10. A syringe pump was used to assist the injection of liquid solution into the CPS in a controlled flow rate (5 ml/min), meanwhile the electrical resistance of CPS was monitored (**Fig. S7**). Inset of **Fig. S7** shows that initially the electrical resistance decreases dramatically, much lower than that of CPS only. With the continuous invasion of the liquid solution into porous spaces of CPS where biomarker (BSA, RBC, or *E. coli*) contacts MWCNTs, the electrical resistance shows an increase. Because of the nature of the superhydrophobicity of CPS, the invaded liquid solution will be drained out spontaneously while leaving RBCs adhered to MWCNTs. Eventually the electrical resistance reaches stable once the liquid solution fully transports across porous spaces of CPS and drains away. This stable electrical resistance shows an apparent decrease compared with that of PDMS sponge only, suggesting the adhesion of RBCs to MWCNTs of CPS [37]. **Fig. 3a** plots the relative change of electrical resistance of CPS at stable stage after a complete flow of liquid with a series of RBC compared with that of CPS only. With the increasing of RBCs, the number of RBC in contact with MWCNTs would be large, and a severe drop of electrical resistance is obtained. Similar results are also obtained when the liquid solution with *E. coli* and BSA flows across CPS and drains out, as shown in **Fig. S8a**. We further define the

electrical resistance signal-to-noise ratio to quantify the sensing sensitivity of CPS to these biomarkers. A large ratio suggests a large measurement noise and low sensing accuracy to biomarkers of CPS. For example, consider the ratio of 3 which is the typical standard in clinical testing [38, 39], the results show that the limit of detection (LOD) of the CPS reaches as low as 10^5/L for RBCs (Fig. 3a), 3.4×10^4 CFU/ml for *E. coli* (Fig. S8a left), and 15 pM for BSA (Fig. S8a right), which is comparable to commercially available biosensors such as Combur-Test® strip from Roche (LOD = 5×10^6/L for RBCs, 600 mg/ml or 9 pM for BSA) [40], and allows examining *E. coli* in the diagnosis of a urinary tract infection (UTI) in a great accuracy [41]. The sensing sensitivity also depends on the dimensional sizes of biomarkers, and smaller biomarkers possess an intensive interaction with MWCNTs per unit, thus leading to higher sensitivity in BSA (~10 nm, versus 1 um for RBCs, versus 10 um for *E. Coli*).

To investigate the sensing sensitivity of CPS to biomarkers in response to mechanical compression, CPS was first deformed under a uniaxial compression strain and then the liquid solution with biomarker were infiltrated by following the same procedure as that in Fig. 3a. For CPS after a full flow of RBC solution, the normalized electrical resistance at the stable stage by that measurement at zero compression strain is plotted in **Fig. 3b**. It shows an increase with the increasing of compression strain yet remains approximately the same when the compression strain reaches 50%. The similar results are also observed on CPS with BSA and *E. Coli*, as shown in **Fig. S8b**, suggesting an enhanced sensing sensitivity of CPS by mechanical compression. This enhancement attributes to a local distribution densification of MWCNTs on compressed CPS that increases the unit contact area between biomarkers and MWNCTs, similar to the increase of electrical conductance under compression in Fig. 2c. **Fig. 3c** shows the densification mechanism of CPS upon mechanical compression. An obvious decrease of pore size in CPS led to the dense compaction of MWCNTs distribution. The densification of MWCNT network facilitates the interactions between biomarkers and MWCNTs, and thus increases the sensitivity of biomarker detection. The microstructural images in **Fig. 3c** further confirm that the MWCNTs was firmly attached on CPS, and the compression of CPS did not influence the sensing sensitivity of CPS, in good agreement with Fig. 2d and Fig. 3b and c. It is envisioned that the sensing sensitivity will decrease at a very high compression that will lead to collapse of porous scaffolds of CPS and does not allow to transport liquid.

Fig. 3d plots the normalized electrical resistance of CPS for sensing solutions with different concentration of biomarkers. The resistance increases with the increasing of biomarkers' concentration in solution and eventually reaches a constant. The increased

resistance indicates an increased quantities of biomarkers sensed by MWCNTs, while the ultimate constant resistance implies the saturation of sensing capacity of MWCNTs to biomarkers, where the critical concentration of biomarkers is referred to the minimum concentration of sensing biomarkers by CPS. Under 40% compression strain, the critical concentration decreases, suggesting that the mechanical compression to CPS improves the sensing capability to biomarkers. Besides, given the same compression strain to CPS (40% in Fig. 3d), the comparison shows that the sensing capability improvement depends on the size of biomarkers. The larger biomarkers are, the more sensing attraction to MWCNTs is, which agrees with the most significant improvement of *E. coli* in comparison with BSA and RBCs. The compressed CPS with local condensed distributions of MWCNTs improves contact areas of MWCNTs with solutions and thus benefits the early sensing of biomarkers, similar to the mechanism of enhanced sensitivity in Fig. 3b.

3.3 Device integration, quantitative measurement and calibration

With the fabrication of CPS and their fundamental sensing mechanism in response to mechanical compression, we integrated it with a portable platform for developing a portable microfluidic device, as shown in the inset of **Fig. 4a**. It consists of three sections: inlet section, testing zone, and outlet chamber. The testing zone can be designed with different dimensional sizes so as to achieve different levels of compression to CPS upon implementation that will benefit the sensing to biomarkers (**Fig. S9**). Besides, the testing zone was designed rectangle with rounded sides to achieve close contacts between compressed CPS and frame that will help prevent leakage of biomarker solution from the Poisson's effect on CPS deformation and ensure its full flow across CPS. The top surface of the frame was sealed with a thin PDMS film and inlets were open to air for accepting the testing biomarker solution (**see Materials and Methods**). In test, urine sample was dropped in one inlet, while the unselected other two inlets were blocked with a solid PDMS bar. After that, pressing and releasing the thin PDMS film on top of the outlet chamber allowed liquid drop being pushed by the atmospheric pressure from inlet to outlet through CPS in the selected channel (**see Materials and Methods**). Fig. 4a shows a higher compression ratio leads to a higher sensitivity, in good consistency with that in Fig. 3b.

Because the sensing mechanism is the physical interaction between biomarkers and MWCNTs in CPS, and the removal of biomarkers will allow the repeated use of CPS. To demonstrate the reusability of CPS, the used CPS was taken out from the testing zone and exposed to sun light that will deactivate biomarkers [42, 43]. For example, the CPS was first

tested with BSA at 15 pM, where the electrical resistance at the measurement stable state was recorded, and then exposed under sun light. **Fig. 4b** plots the normalized electrical resistance of the CPS with the number of testing/sun exposure cycle. CPS shows a rapid degradation with a dramatic decrease of electrical resistance after use. By contrast, after 20 min exposure to sun light, the electrical resistance achieves a full recovery even after more than 10 times of usage, demonstrating the great reusability of CPS devices by sunlight exposure.

3.4 *Ex vivo* urine analysis of mouse disease models

To valid the sensitivity of CPS devices, ex vivo test was conducted with nephrotoxic serum (NTS)-induced nephritis of mice, as illustrated in **Figure S10a**. The urine samples were collected from baseline (before injection), early period group (day 3 after injection), and nephritis group (day 9 after injection). **Figure 5a** shows the measured electrical resistance of urine samples with our CPS device. An obvious increase is observed with the progression of disease, suggesting the successful sensing of glucose in urine, in great agreement with biochemical measurement of albumin with an ELISA kit. Experiments on urine of streptozotocin-induced diabetic mice were also conducted, as illustrated in **Figure S10b**. Different from nephritis mice group, an islet transplant surgery was performed on diabetic mice and urine samples were collected 30 days after surgery. The well agreement between measured glucose by CPS device and a commercial glucose kit, as shown in **Figure 5b**, further confirms the potential application in real time monitor of biomarkers both during the incidence and after treatment.

4. Conclusions

In summary, we have reported an electrical sensing based, soft porous PDMS scaffolds enabled, cellular microfluidic device and demonstrated its applications in sensing common biomarkers in urine in a fast and accuracy manner. A swelling/shrinking-induced decoration of MWCNTs onto porous PDMS scaffolds is developed to obtain electrically conductive PDMS sponges, referred to as CPS. The CPS exhibits an excellent electrical conductivity and surface superhydrophobicity. These properties remain unchanged after cyclic mechanical compressions to CPS, which confirms the decoration stability and adhesion strength of MWCNTs on PDMS scaffolds. Systematical studies of CPS in response to artificial urine samples with a series of biomarker concentrations including red blood cells (RBCs), *Escherichia coli* (*E. coli*), and bovine serum albumin (BSA) demonstrate a fast responsive capability to sense biomarkers in a high accuracy. In particular, CPS under a mechanical

compression shows enhancements of both sensing accuracy and capability to flow solutions with a low biomarker concentration. The CPS is implemented into a portable platform in the design of cellular microfluidic devices, and the design of testing zones with a customizable-size feature in the devices achieves to tune CPS sensing performance through a mechanical means. *Ex vivo* animal urine tests with nephritis and diabetes demonstrate the applications of CPS enabled portable devices for urinalysis in agreement with existing biochemical tests. The swelling-induced decoration of MWCNTs on porous PDMS scaffolds reported here offers a robust route of coating nanomaterials onto soft materials for potentially applications in the fabrication of low-cost surface wetting structures, electronics, and sensors. The concept and design of the electrically conductive CPS enabled microfluidic devices will enable quantitative monitoring and diagnosis of body fluid by integrating wearable electronics and microfluidic biomedical devices and is also open for the exploration of remote controllable ways with the implementation of environmentally responsive smart materials such as optical, magnetic and acoustic field, beyond the mechanical programmable manner.

References

[1] E. Holmes, I.D. Wilson, J.K. Nicholson, Metabolic phenotyping in health and disease, Cell 134(5) (2008) 714-717.

[2] N.A. Brunzel, Fundamentals of Urine and Body Fluid Analysis-E-Book, Elsevier Health Sciences2016.

[3] J.Y. Yang, R.D. Sarwal, T.K. Sigdel, I. Damm, B. Rosenbaum, J.M. Liberto, C. Chan-On, J.M. Arreola-Guerra, J. Alberu, F. Vincenti, A urine score for noninvasive accurate diagnosis and prediction of kidney transplant rejection, Science Translational Medicine 12(535) (2020) eaba2501.

[4] H. Markus, J. Zhao, T. Contente-Cuomo, M.D. Stephens, E. Raupach, A. Odenheimer-Bergman, S. Connor, B.R. McDonald, B. Moore, E. Hutchins, Analysis of recurrently protected genomic regions in cell-free DNA found in urine, Science Translational Medicine 13(581) (2021) eaaz3088.

[5] M. Magruder, A.N. Sholi, C. Gong, L. Zhang, E. Edusei, J. Huang, S. Albakry, M.J. Satlin, L.F. Westblade, C. Crawford, Gut uropathogen abundance is a risk factor for development of bacteriuria and urinary tract infection, Nature Communications 10(1) (2019) 1-9.

[6] B. Foxman, The epidemiology of urinary tract infection, Nature Reviews Urology 7(12) (2010) 653-660.

[7] G.J. Wise, P.N. Schlegel, Sterile pyuria, New England Journal of Medicine 372(11) (2015) 1048-1054.

[8] M. Jeun, S. Park, Y. Kim, J. Choi, S.H. Song, I.G. Jeong, C.S. Kim, K.H. Lee, Self-normalized detection of ANXA3 from untreated urine of prostate cancer patients without digital rectal examination, Advanced Healthcare Materials 6(17) (2017) 1700449.

[9] H. Karlsen, T. Dong, Biomarkers of urinary tract infections: state of the art, and promising applications for rapid strip-based chemical sensors, Analytical Methods 7(19) (2015) 7961-7975.

[10] A.P. Acharya, K.M. Theisen, A. Correa, T. Meyyappan, A. Apfel, T. Sun, T.V. Tarin, S.R. Little, An Inexpensive, Point-of-Care Urine Test for Bladder Cancer in Patients Undergoing Hematuria Evaluation, Advanced Healthcare Materials 6(22) (2017) 1700808.

[11] R. Hiraoka, K. Kuwahara, Y.-C. Wen, T.-H. Yen, Y. Hiruta, C.-M. Cheng, D. Citterio, Based Device for Naked Eye Urinary Albumin/Creatinine Ratio Evaluation, ACS Sensors 5(4) (2020) 1110-1118.

[12] H. Liu, Z. Li, R. Shen, Z. Li, Y. Yang, Q. Yuan, Point-of-Care Pathogen Testing Using Photonic Crystals and Machine Vision for Diagnosis of Urinary Tract Infections, Nano Letters 21(7) (2021) 2854-2860.

[13] G.T. Smith, N. Dwork, S.A. Khan, M. Millet, K. Magar, M. Javanmard, A.K.E. Bowden, Robust dipstick urinalysis using a low-cost, micro-volume slipping manifold and mobile phone platform, Lab on a Chip 16(11) (2016) 2069-2078.

[14] X. Lei, X. Xu, L. Liu, H. Kuang, L. Xu, C. Hao, C. Xu, Rapid quantitative determination of fentanyl in human urine and serum using a gold-based immunochromatographic strip sensor, Journal of Materials Chemistry B 8(37) (2020) 8573-8584.

[15] U.M. Jalal, G.J. Jin, J.S. Shim, Paper–plastic hybrid microfluidic device for smartphone-based colorimetric analysis of urine, Analytical Chemistry 89(24) (2017) 13160-13166.

[16] H. Li, E. Shkolyar, J. Wang, S. Conti, A.C. Pao, J.C. Liao, T.-S. Wong, P.K. Wong, SLIPS-LAB—A bioinspired bioanalysis system for metabolic evaluation of urinary stone disease, Science Advances 6(21) (2020) eaba8535.

[17] Z. Li, Y. Wang, J. Wang, Z. Tang, J.G. Pounds, Y. Lin, Rapid and sensitive detection of protein biomarker using a portable fluorescence biosensor based on quantum dots and a lateral flow test strip, Analytical Chemistry 82(16) (2010) 7008-7014.

[18] A.A. Burns, J. Vider, H. Ow, E. Herz, O. Penate-Medina, M. Baumgart, S.M. Larson, U. Wiesner, M. Bradbury, Fluorescent silica nanoparticles with efficient urinary excretion for nanomedicine, Nano Letters 9(1) (2009) 442-448.

[19] D. Yan, Y. Lou, Y. Yang, Z. Chen, Y. Cai, Z. Guo, H. Zhan, B. Chen, Dye-Modified Metal–Organic Framework as a Recyclable Luminescent Sensor for Nicotine Determination in Urine Solution and Living Cell, ACS Applied Materials & Interfaces 11(50) (2019) 47253-47258.

[20] S. Milo, F.B. Acosta, H.J. Hathaway, L.A. Wallace, N.T. Thet, A.T.A. Jenkins, Development of an infection-responsive fluorescent sensor for the early detection of urinary catheter blockage, ACS Sensors 3(3) (2018) 612-617.

[21] H. Amer, M. Fidler, M. Myslak, P. Morales, W. Kremers, T. Larson, M. Stegall, F. Cosio, Proteinuria after kidney transplantation, relationship to allograft histology and survival, American Journal of Transplantation 7(12) (2007) 2748-2756.

[22] B.R. Hemmelgarn, B.J. Manns, A. Lloyd, M.T. James, S. Klarenbach, R.R. Quinn, N. Wiebe, M. Tonelli, A.K.D. Network, Relation between kidney function, proteinuria, and adverse outcomes, JAMA 303(5) (2010) 423-429.

[23] R. Sha, N. Vishnu, S. Badhulika, MoS2 based ultra-low-cost, flexible, non-enzymatic and non-invasive electrochemical sensor for highly selective detection of uric acid in human urine samples, Sensors and Actuators B: Chemical 279 (2019) 53-60.

[24] Z. Sun, C. Han, M. Song, L. Wen, D. Tian, H. Li, L. Jiang, Fabrication of Cysteine-Responsive Biomimetic Single Nanochannels by a Thiol-yne Reaction Strategy and Their Application for Sensing in Urine Samples, Advanced Materials 26(3) (2014) 455-460.

[25] X. Hui, M. Sharifuzzaman, S. Sharma, X. Xuan, S. Zhang, S.G. Ko, S.H. Yoon, J.Y. Park, High-Performance Flexible Electrochemical Heavy Metal Sensor Based on Layer-by-Layer Assembly of Ti3C2T x/MWNTs Nanocomposites for Noninvasive Detection of Copper and Zinc Ions in Human Biofluids, ACS Applied Materials & Interfaces 12(43) (2020) 48928-48937.

[26] L. Lacerda, A. Soundararajan, R. Singh, G. Pastorin, K.T. Al-Jamal, J. Turton, P. Frederik, M.A. Herrero, S. Li, A. Bao, Dynamic imaging of functionalized multi-walled carbon nanotube systemic circulation and urinary excretion, Advanced Materials 20(2) (2008) 225-230.

[27] S. Jeong, J. Park, D. Pathania, C.M. Castro, R. Weissleder, H. Lee, Integrated magneto–electrochemical sensor for exosome analysis, ACS Nano 10(2) (2016) 1802-1809.

[28] M.K. Nguyen, W.N. Su, B.J. Hwang, A Plasmonic Coupling Substrate Based on Sandwich Structure of Ultrathin Silica-Coated Silver Nanocubes and Flower-Like Alumina-Coated Etched Aluminum for Sensitive Detection of Biomarkers in Urine, Advanced Healthcare Materials 6(10) (2017) 1601290.

[29] M. Ghoneim, A. Nguyen, N. Dereje, J. Huang, G. Moore, P. Murzynowski, C. Dagdeviren, Recent progress in electrochemical pH-sensing materials and configurations for biomedical applications, Chemical Reviews 119(8) (2019) 5248-5297.

[30] P. Ledezma, P. Kuntke, C.J. Buisman, J. Keller, S. Freguia, Source-separated urine opens golden opportunities for microbial electrochemical technologies, Trends in Biotechnology 33(4) (2015) 214-220.

[31] L. Mu, I.A. Droujinine, N.K. Rajan, S.D. Sawtelle, M.A. Reed, Direct, rapid, and label-free detection of enzyme–substrate interactions in physiological buffers using CMOS-compatible nanoribbon sensors, Nano Letters 14(9) (2014) 5315-5322.

[32] S.-J. Choi, T.-H. Kwon, H. Im, D.-I. Moon, D.J. Baek, M.-L. Seol, J.P. Duarte, Y.-K. Choi, A polydimethylsiloxane (PDMS) sponge for the selective absorption of oil from water, ACS Applied Materials & Interfaces 3(12) (2011) 4552-4556.

[33] J.S. Sun-sang, Y. Ge, C. Dai, H. Wang, S.M. Fu, R. Sharma, Y.S. Hahn, J. Yu, T.H. Le, M.D. Okusa, Dependence of glomerulonephritis induction on novel intraglomerular alternatively activated bone marrow–derived macrophages and Mac-1 and PD-L1 in lupus-prone NZM2328 mice, The Journal of Immunology 198(7) (2017) 2589-2601.

[34] G.S. Braun, Y. Nagayama, Y. Maruta, F. Heymann, C.R. van Roeyen, B.M. Klinkhammer, P. Boor, L. Villa, D.J. Salant, U. Raffetseder, IL-6 trans-signaling drives murine crescentic GN, Journal of the American Society of Nephrology 27(1) (2016) 132-142.

[35] B. Smeets, S. Uhlig, A. Fuss, F. Mooren, J.F. Wetzels, J. Floege, M.J. Moeller, Tracing the origin of glomerular extracapillary lesions from parietal epithelial cells, Journal of the American Society of Nephrology 20(12) (2009) 2604-2615.

[36] P. Chhabra, K. Schlegel, M.D. Okusa, P.I. Lobo, K.L. Brayman, Naturally occurring immunoglobulin M (nIgM) autoantibodies prevent autoimmune diabetes and mitigate inflammation after transplantation, Annals of Surgery 256(4) (2012).

[37] Y. Yang, K. Gupta, K.L. Ekinci, All-electrical monitoring of bacterial antibiotic susceptibility in a microfluidic device, Proceedings of the National Academy of Sciences 117(20) (2020) 10639-10644.

[38] B. Pérez-López, A. Merkoçi, Magnetic nanoparticles modified with carbon nanotubes for electrocatalytic magnetoswitchable biosensing applications, Advanced Functional Materials 21(2) (2011) 255-260.

[39] A. Shrivastava, V.B. Gupta, Methods for the determination of limit of detection and limit of quantitation of the analytical methods, Chronicles of young scientists 2(1) (2011) 21-25.

[40] J. Penders, T. Fiers, J.R. Delanghe, Quantitative evaluation of urinalysis test strips, Clinical Chemistry 48(12) (2002) 2236-2241.

[41] L.E. Nicolle, Uncomplicated urinary tract infection in adults including uncomplicated pyelonephritis, Urologic Clinics of North America 35(1) (2008) 1-12.

[42] L.W. Sinton, C.H. Hall, P.A. Lynch, R.J. Davies-Colley, Sunlight inactivation of fecal indicator bacteria and bacteriophages from waste stabilization pond effluent in fresh and saline waters, Applied and Environmental Microbiology 68(3) (2002) 1122-1131.

[43] C.C. Wang, K.A. Prather, J. Sznitman, J.L. Jimenez, S.S. Lakdawala, Z. Tufekci, L.C. Marr, Airborne transmission of respiratory viruses, Science 373(6558) (2021) eabd9149.
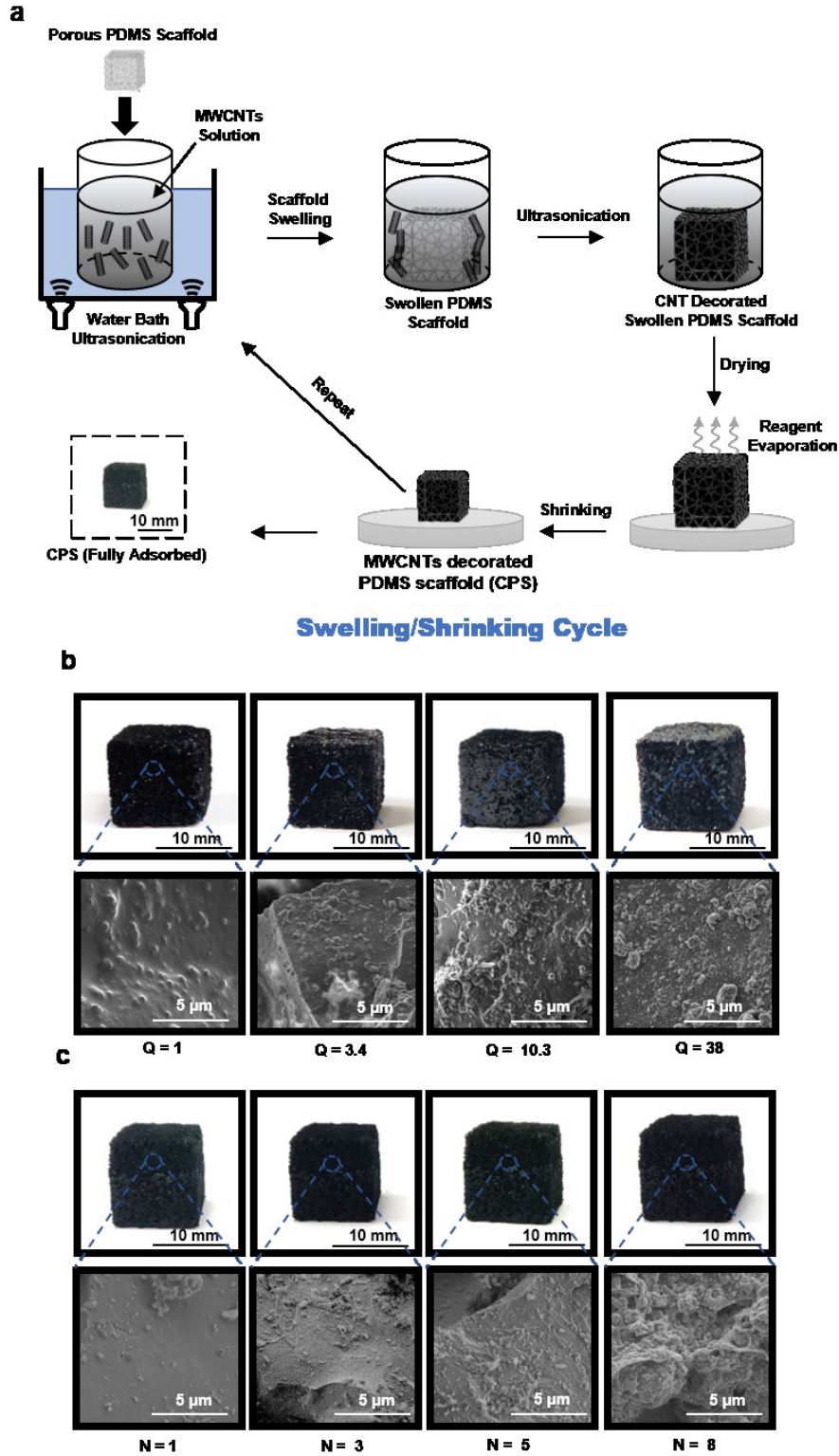
Fig. 1. Fabrication of electrically conductive porous PDMS scaffolds with decoration of multiwalled carbon nanotubes (MWCNTs). (a) Schematic illustrations of preparing MWCNTs decorated PDMS scaffolds (CPS) through cyclic swelling/shrinking-induced MWCNTs adsorption. Dashed box shows an optical image of CPS with fully absorbed MWCNTs after seven swelling/shrinking cycles. Optical (top) and SEM (bottom) images of CPS structures obtained with (b) different swelling ratio Q in the reagents and (c) different swelling/shrinking cycles.

16
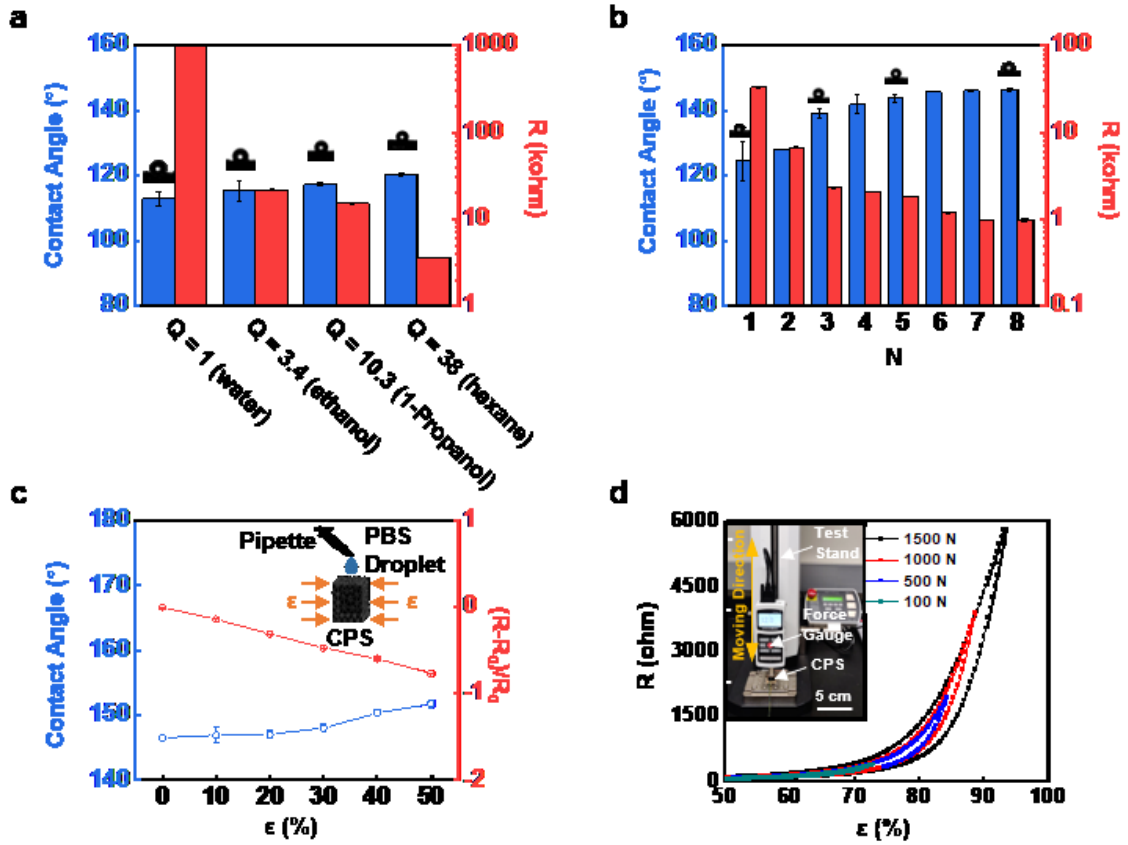
Fig. 2. Electrical and wetting properties of CPS. (a) Effect of swelling ratio on surface wettability via contact angle measurement and electrical resistance of CPS. CPS swollen in water is dielectric because the swelling ratio (Q) of water is 1 (no swelling). (b) Variation of contact angle and resistance of CPS with adsorption cycles (N). Insets in (a) and (b) are optical images of measuring contact angle of liquid droplet on CPS. (c) Contact angle and electrical resistance of CPS in response to a mechanical compression ε. Inset shows the schematic of measuring the contact angle, where PBS droplet was dropped onto the top surface of a CPS with a pipette after a mechanical compression ε was applied. (d) Dynamic response of electrical resistance of CPS under a compression-rehabilitation cycle with different compression forces. Inset shows the optical image of experimental measurement system. The regent solution was hexane with Q of 38 in (b-d)
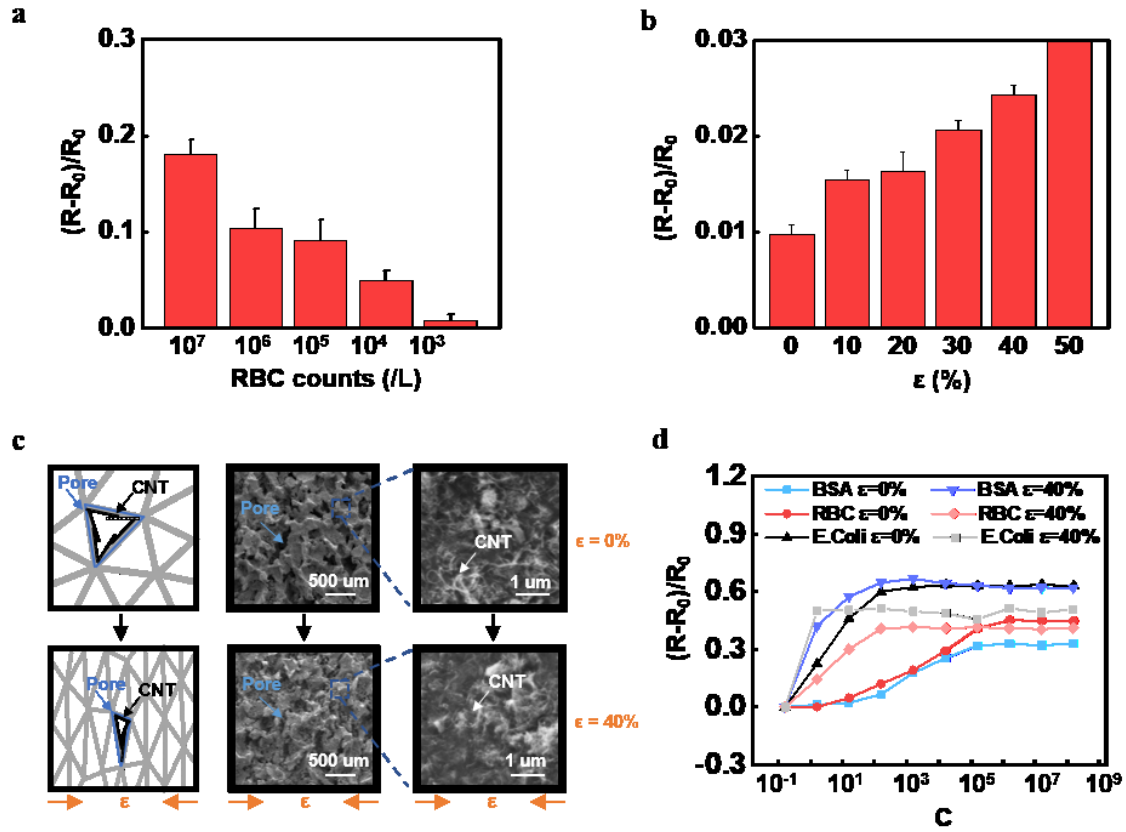
Fig. 3. Electrical sensing properties of CPS to biomarkers. (a) Normalized electrical resistance of CPS in response to liquid solution transport inside with different counts of red blood cell (RBC). R_0 and R are resistance of CPS before and after injection of RBC solution, respectively. (b) Normalized electrical resistance of CPS to RBC solution (10^7/L) subjected to a mechanical compression strain, ε. (c) Schematics (left) and SEM images (right) of CPS structural morphologies before and after applying a 40% mechanical compression strain. (d) Comparison of normalized electrical resistance of CPS to liquid solutions with different biomarkers without and with a mechanical strain.
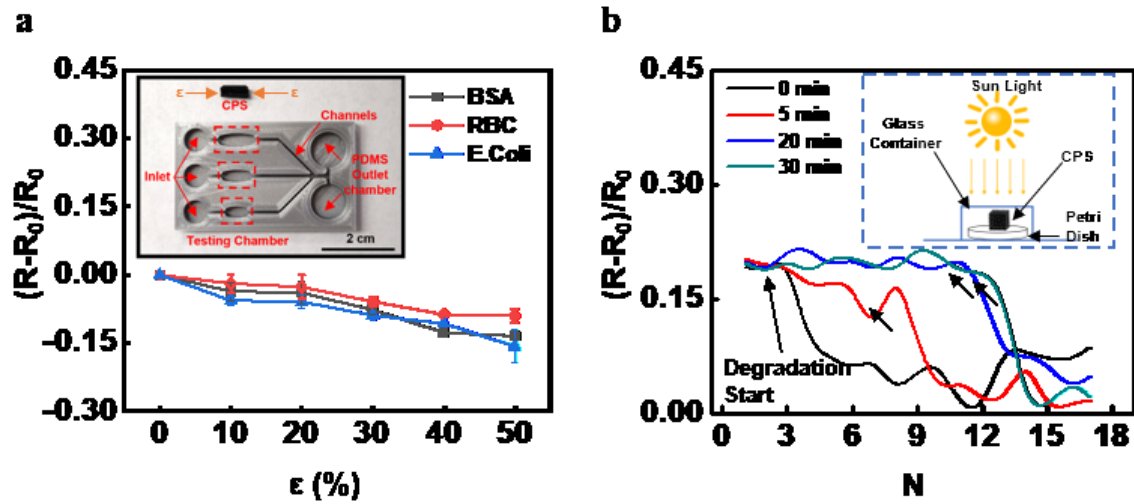
Fig. 4. Integration and characterization of CPS based cellular microfluidic device. (a) Measured electrical resistance in the microfluidic device when a biomarker solution (BSA, RBCs, or *E. Coli*) flows through CPS sensor whose mechanical deformation can be programmed by customizing its size when placing in the testing chamber. Inset shows the optical image of the device capable of being integrated with three CPS sensor elements. (b) Reusability characterization of CPS sensor element in the device by exposing to sunlight, where BSA solution with 15 pM was employed. Inset shows the schematic of sunlight expose experimental setup.
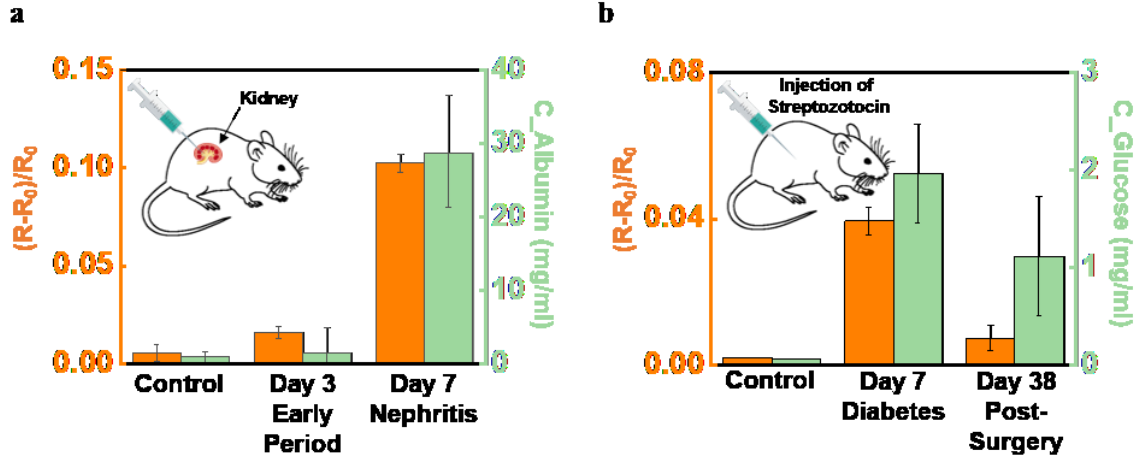
Fig. 5. *Ex vivo* **assessment of the CPS based microfluidic device. (a)** Comparison of measured electrical resistance by the CPS device and clinical testing results from ELISA among control group, early period (3-days), and nephritis (7-days) urine samples with albumin. Inset shows the inducement of nephritis by nephrotoxic serum (NTS). **(b)** Comparison of measured electrical resistance by the CPS device and clinical testing results from a commercial kit among control group, diabetes induced, and after-treatment urine samples with glucose. Inset shows the induction of disbete by the injection of streptozotocin.